



HAL
open science

Optoelectronic properties of a self-assembling rigidly-linked BF₂-curcuminoid bichromophore

Claire Tonnelé, Manon Catherin, Michel Giorgi, Gabriel Canard, David Casanova, Frédéric Castet, Elena Zaborova, Frédéric Fages

► To cite this version:

Claire Tonnelé, Manon Catherin, Michel Giorgi, Gabriel Canard, David Casanova, et al.. Optoelectronic properties of a self-assembling rigidly-linked BF₂-curcuminoid bichromophore. *Dyes and Pigments*, 2022, 207, pp.110677. 10.1016/j.dyepig.2022.110677 . hal-03778198

HAL Id: hal-03778198

<https://amu.hal.science/hal-03778198>

Submitted on 15 Sep 2022

HAL is a multi-disciplinary open access archive for the deposit and dissemination of scientific research documents, whether they are published or not. The documents may come from teaching and research institutions in France or abroad, or from public or private research centers.

L'archive ouverte pluridisciplinaire **HAL**, est destinée au dépôt et à la diffusion de documents scientifiques de niveau recherche, publiés ou non, émanant des établissements d'enseignement et de recherche français ou étrangers, des laboratoires publics ou privés.

Optoelectronic properties of a self-assembling rigidly-linked BF₂-curcuminoid bichromophore

Claire Tonnelé^{a,†}, Manon Catherin^{b,†}, Michel Giorgi^c, Gabriel Canard^b, David Casanova^{a,d,*},
Frédéric Castet^{e,**}, Elena Zaborova^{b,***}, Frédéric Fages^{b,****}

^a *Donostia International Physics Center (DIPC), Paseo Manuel de Lardizabal 4, 20018 Donostia, Euskadi (Spain)*

^b *Aix Marseille Univ, CNRS, CINaM UMR 7325, AMUtech, Campus de Luminy, Case 913, 13288 Marseille (France)*

^c *Aix Marseille Univ, CNRS, Centrale Marseille, FSCM, Spectropole, Marseille, France*

^d *IKERBASQUE – Basque Foundation for Science, 48009 Bilbao, Euskadi, Spain*

^e *Univ. Bordeaux, CNRS, Bordeaux INP, ISM, UMR 5255, F-33405 Cedex Talence, France*

[†]Dr C. Tonnelé and M. Catherin contributed equally to this work.

*Corresponding author

** Corresponding author

*** Corresponding author

**** Corresponding author

Email addresses: david.casanova@ehu.eus (D. Casanova), frederic.castet@u-bordeaux.fr (F.Castet), elena.zaborova@univ-amu.fr (E. Zaborova), frederic.fages@univ-amu.fr (F. Fages).

ARTICLE INFO

Keywords:

Quadrupolar chromophores

Curcuminoids

Bichromophoric molecules

Dye aggregation

DFT studies

ABSTRACT

We describe the synthesis and spectroscopic study of the bichromophoric molecule **DA-meso** consisting of two boron difluoride curcuminoid (BF₂-curcuminoid) units tethered by the rigid diacetylenic bridge. This structural feature imparts the quadrupolar-like **DA-meso** with a strong ability to self-assemble in solution, which induces a profound change in the optical properties. The UV-vis absorption spectrum of the aggregate is characterized by the appearance of a redshifted band at low energy and its fluorescence emission occurs in the near infrared ($\lambda_{\text{max}} = 700$ nm) with a low quantum yield (5 %). This is in contradiction with the strong emission expected for J-aggregates considering the Frenkel exciton model. From concentration-dependent UV-vis absorption spectroscopy we demonstrate the formation of a dimer composed of four BF₂-curcuminoid units. Single-crystal X-ray diffraction structure analysis and in-depth quantum chemical calculations based on density functional theory (DFT) and subsequent decomposition of the electronic excited states on a diabatic basis enable to discuss the geometry of the **DA-meso** dimer, and to establish the presence of excited states close in energy to that of the unperturbed monochromophore, which are not predicted by the classical Frenkel exciton model. Different dimer structures characterized by π -stacks of two and up to four chromophores are investigated, in which low-lying excited states with

vanishing oscillator strength are found to be redshifted with respect to the lowest-energy allowed state of the aggregate. From these experimental and theoretical data, the spectral features of the **DA-meso** dimer are rationalized by considering the formation of a “non-fluorescent J-aggregate”, illustrating the trend in non-Kasha behavior observed for quadrupolar-like dyes.

1. Introduction

The understanding of solid-state optical and electronic properties of dye molecules and organic semiconductors is key to improving the performance of functional materials for electronic, photonic, nonlinear optic, and photovoltaic applications [1-14]. Neutral electronic excitations, known as Frenkel excitons, play a fundamental role in electronic absorption, luminescence emission, and charge generation processes taking place in molecular aggregates. This is especially the case for polycyclic (hetero)aromatic hydrocarbons such as oligoacenes and perylene derivatives characterized by weak permanent ground-state and excited-state dipole moments. In this case, the $S_1 \leftarrow S_0$ transition displays no significant intramolecular charge transfer (intra-CT) contribution, making the associated transition dipole moment poorly sensitive to the environment. As a result, a satisfactory description for the change in optical properties when passing from the isolated to the aggregated molecules is provided by the long-range Coulombic interaction coupling between transition dipoles, which is itself determined by the spatial arrangement of interacting molecules in the aggregate [15]. Within the Kasha model, based on the Frenkel exciton theory, red and blue shifts of the electronic absorption spectra are usually considered as characteristic spectral signatures of the standard J- and H-aggregates, respectively.

Unlike apolar acenes, dipolar D- π -A and polarizable quadrupolar-like D- π -A- π -D (or A- π -D- π -A) chromophores, where D and A denote electron donor and acceptor subunits, respectively, bridged by a π -conjugated moiety, display an intriguing behavior. Indeed, large deviations from the Frenkel exciton model have been noticed for a variety of such molecular systems in the solid state, including multipolar V-shaped chromophores and squaraines [16-22]. Dipolar and quadrupolar π -conjugated molecules constitute a topical class of chemical structures on which to base delayed fluorescence (DF) emitters and donors or acceptors for bulk heterojunction solar cells for example [23-31]. In view of their photonic and electronic

applications, it is therefore crucial to understand the properties of this class of molecules in the solid state.

The non-Kasha behavior of dipolar D- π -A and polarizable D- π -A- π -D chromophores largely stems from the intra-CT nature of the $S_1 \leftarrow S_0$ transition inducing significant changes in electronic distribution and dipole moment in the excited state. In other terms, the transition dipole moment of polar and polarizable dyes is much more sensitive to intermolecular interactions than that of apolar chromophores, and acutely feels the electrostatic potential generated by neighboring molecules [16,19,32,33]. The Frenkel exciton picture overlooks these features and is therefore insufficient to explain the observed anomalous spectral shifts and band shapes for the head-to-tail (J) and card-pack (H) arrangements for example. Furthermore, D and A fragments of adjacent D- π -A and D- π -A- π -D dyes in the solid state can exhibit dense aggregation modes with close contacts between D and A moieties of interacting molecules. Such short-range interactions can promote the formation of low-energy intermolecular charge transfer (inter-CT) states resulting from the dissociation of Frenkel excitons into pairs of charge carriers localized at different molecules [34-36]. In this sense, Spano has outlined the theoretical grounds to rationalize the effect of inter-CT interactions on the optical properties of dye aggregates [37].

Recently, we have reported the photophysical properties of a series of boron difluoride (BF_2) complexes of curcuminoid derivatives (BF_2 -curcuminoids) in solution- and solid-state [38-43]. These molecules have a D- π -A- π -D structure comprising a dioxaborine (DOB) ring as A motif and a variety of terminal D groups have been considered. The triphenylamine (TPA) D unit has been shown to endow the **BF2** compound (Chart 1) with DF emission in the solid state as due to the participation of dark singlet and triplet inter-CT states interconverting with the emitting intra-CT singlet state [44]. Despite significant intermolecular π -stacking interactions in the crystal, the shape of the UV-vis absorption spectra of solid-state TPA-

containing BF₂-curcuminoids did not exhibit the profound changes generally expected for excitonically coupled chromophores [38,39,44]. In contrast, the solid-state absorption spectra of related chromophores with two *para*-methoxyphenyl (PMP) D subunits as in **R-Me** (Chart 1) were found to be strongly affected, showing the appearance of a redshifted shoulder at low energy that suggests the possible formation of J-aggregates [21]. However, **R-Me** showed a considerably redshifted fluorescence with respect to the emission in solution, reaching a maximum beyond 700 nm and having a low quantum yield Φ_f of 5 %, in contradiction with the strong emission expected for J-aggregates within the Frenkel exciton model. Moreover, no DF emission could be detected in the case of PMP-containing BF₂-curcuminoids.

In a previous attempt to rationalize the behavior of PMP-containing BF₂-curcuminoids, we investigated different covalently-tethered bichromophoric dyes in which two BF₂-curcuminoid units were linked by a flexible polymethylenic chain [22,45]. Although these model compounds provided interesting experimental and theoretical insights into the electronic and photophysical properties of loosely interacting BF₂-curcuminoid units, the data did not reproduce the spectral feature on the red side of the UV-vis absorption band and the considerably redshifted and weak fluorescent emission, both characteristic of tightly aggregated BF₂-curcuminoid dyes in the solid state, e.g., in **R-Me** nanoparticles [21]. Therefore, there is a need for building aggregate models having a geometry and a size more representative of the solid-state arrangements. In this context, we report the synthesis and aggregation behavior of **DA-meso** in which a rigid diacetylene linker bridges two BF₂-curcuminoid units via the phenoxy group on the central (*meso*) position of each curcuminoid backbone (Chart 1). The choice of the diacetylene spacer has proven successful in a number of studies, including the generation of receptors for organic molecules [46], tweezer molecules [47] and reactive self-assembling building blocks in topochemical photoreactions [48]. The Würthner group used the diacetylene spacer to generate well-defined

dye aggregate structures and, as an example, described recently the spacer-encoded self-assembly of merocyanine H-aggregates composed of π -stacks of up to eight chromophores [49]. In this study, we have investigated the solution-phase self-assembly of **DA-meso** using concentration-dependent UV-vis absorption spectroscopy, single-crystal X-ray diffraction structure analysis and quantum chemical calculations based on density functional theory (DFT). Decomposition of the electronic excited states on a diabatic basis allowed us to gain deep insight into the nature of electronic excited states of the aggregates, in comparison to those of the **R-meso** monochromophoric compound used as reference (Chart 1).

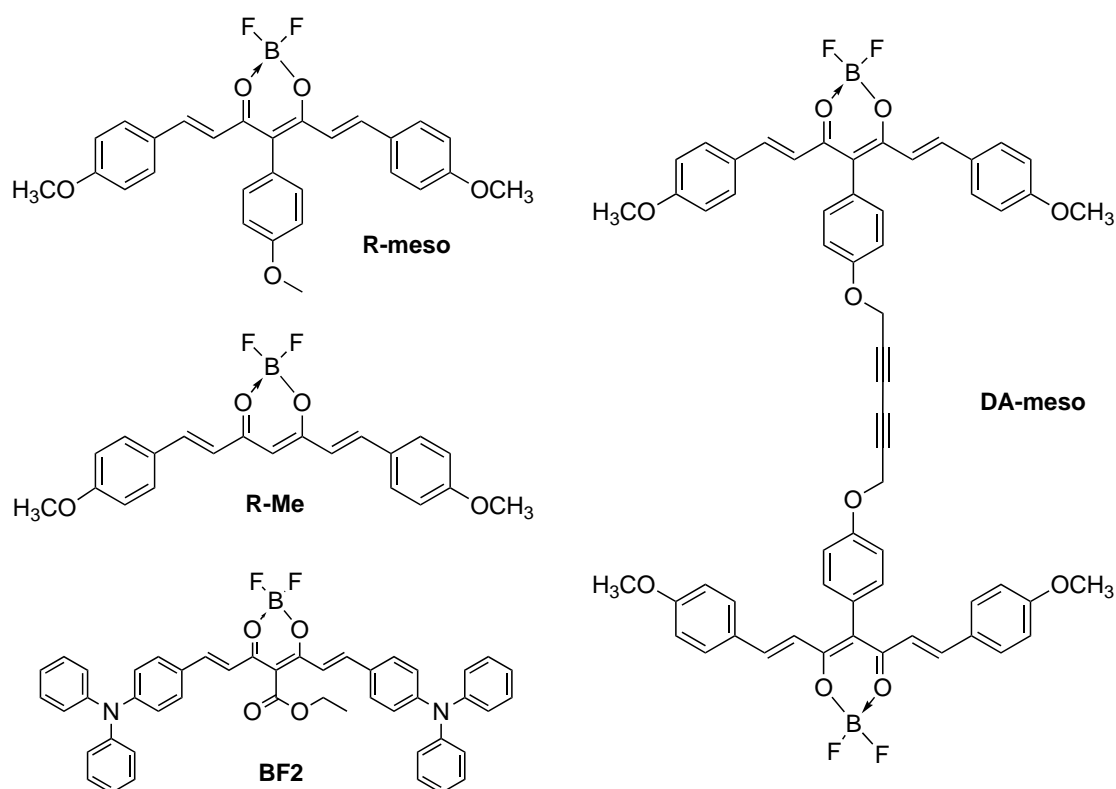


Chart 1.

2. Experimental section

2.1. Materials and general physical measurements

All solvents for synthesis and spectroscopic measurements were of analytic and spectroscopy grades, respectively. NMR spectra were recorded at room temperature on a JEOL JNM ECS 400 (400, 100 and 376 MHz for ^1H , ^{13}C and ^{19}F respectively). Data are given

in parts per million (ppm) and are reported relative to tetramethylsilane (^1H); residual solvent peaks of the deuterated solvents were used as an internal standard. The multiplicity of signals is designated by the following abbreviations: s, singlet; d, doublet; t, triplet. High-resolution mass spectrometry (HR-MS) was performed on a SYNAPT G2 HDMS (Waters) with electrospray ionization (ESI) in the positive mode and time-of-flight (TOF) mass analysis. UV-vis absorption spectra were measured using a dual-beam JASCO V670 spectrophotometer and quartz cuvettes with a path length of 10 cm. Fluorescence and phosphorescence emission spectra were recorded on a FluoroLog-3 (Jobin Yvon HORIBA iHR 320). Cyclic voltammetry was carried out using a BAS 100 Potentiostat (Bioanalytical Systems). A Pt working electrode (diameter 1.6 mm), a Pt counter electrode and a leak-free Ag/AgCl reference electrode of 5 mm diameter were used. Cyclic voltammograms were recorded at a scan rate of $100 \text{ mV}\cdot\text{s}^{-1}$ for solutions of the compounds ($5\times 10^{-4} \text{ M}$) in dichloromethane (DCM) containing *n*-Bu₄NPF₆ (0.1 M) as supporting electrolyte. Ferrocene (Fc) was used as an internal standard. The data were analyzed with BAS100W software (v2.3).

2.2. *Synthesis of DA-meso*

DA-meso was synthesized following the route shown in Scheme 1. Compound **1** was synthesized according to a published procedure [40].

2.2.1. *Compound 2*

BBr₃ (4.85 mL, 1 M solution in DCM) was added dropwise to a solution of compound **1** (200 mg, 0.97 mmol) in DCM (10 mL) maintained at 0 °C. The reaction mixture was stirred at room temperature overnight. The reaction was quenched with water (20 mL) and extracted three times with ethyl acetate (3 x 30 mL). The combined organic layers were dried over anhydrous MgSO₄, filtered and the solvent was removed under vacuum. The crude product was purified on a silica gel column with petroleum ether/ethyl acetate (8/2 v:v) as eluent,

giving **2** as a white powder (141 mg, 79 %). ^1H NMR (400 MHz, CDCl_3) δ (ppm): 7.03 (d, $J = 8.6$ Hz, 2H), 6.85 (d, $J = 8.6$ Hz, 2H), 1.89 (s, 6H). $^{13}\text{C}\{^1\text{H}\}$ NMR (100 MHz, CDCl_3) δ (ppm): 191.4, 155.1, 132.5, 129.4, 115.9, 114.7, 24.3.

2.2.2. Compound 3

A solution of compound **2** (620 mg, 3.23 mmol), 3-bromo-1(trimethylsilyl)-1-propyne (792 μL , 4.85 mmol) and potassium carbonate (536 mg, 3.88 mmol) in acetone (5 mL) was refluxed for 4 h. After filtration and solvent evaporation, the residue was taken into ethyl acetate (100 mL). The organic phase was washed with brine (30 mL), water (30 mL), and dried over anhydrous MgSO_4 . After filtration, the solvent was removed under vacuum and the crude product was purified on a silica gel column with cyclohexane/DCM (3/7 v:v) as eluent, giving product **3** as a yellow oil (498 mg, 51 %). ^1H NMR (400 MHz, CDCl_3) δ (ppm): 7.08 (d, $J = 8.8$ Hz, 2H), 6.98 (d, $J = 8.7$ Hz, 2H), 4.07 (s, 2H), 1.89 (s, 6H), 0.17 (s, 9H). $^{13}\text{C}\{^1\text{H}\}$ NMR (100 MHz, CDCl_3) δ (ppm): 191.4, 157.2, 132.2, 130.0, 115.3, 114.7, 100.0, 93.1, 57.0, 24.3, 0.17.

2.2.3. Compound 4

Compound **3** (500 mg, 1.70 mmol) and B_2O_3 (260 mg, 3.74 mmol) were mixed into ethyl acetate (10 mL) and stirred at 60 $^\circ\text{C}$ for 30 min. A solution of 4-methoxybenzaldehyde (455 μL , 3.74 mmol) and tri-*n*-butyl borate (1.15 mL, 4.25 mmol) in ethyl acetate (10 mL) was added, and the mixture was stirred at 60 $^\circ\text{C}$ for 30 min. Then, *n*-butylamine (84 μL , 0.85 mmol) was added to the solution. A second aliquot of *n*-butylamine (84 μL , 0.85 mmol) was added after 2 h. The reaction mixture was heated overnight. After cooling to room temperature, a solution of diluted hydrochloric acid (10 mL) and water (90 mL) was added and the resulting mixture was stirred for an additional 30 min. The reaction mixture was extracted with ethyl acetate (3 x 100 mL). The organic layer was dried over anhydrous MgSO_4 , and the solvent was removed under vacuum to leave a brown residue. The crude

product was purified on a silica gel column with cyclohexane/DCM (1/1 v:v) as eluent. Compound **4** was obtained as an orange solid (345 mg, 38 %). Mp: 119–120 °C. ¹H NMR (400 MHz, CDCl₃) δ (ppm): 7.65 (d, *J* = 15.7 Hz, 2H), 7.31 (d, *J* = 8.6 Hz, 4H), 7.21 (d, *J* = 8.4 Hz, 2H), 7.05 (d, *J* = 8.5 Hz, 2H), 6.83 (d, *J* = 8.5 Hz, 4H), 6.39 (d, *J* = 15.6 Hz, 2H), 4.78 (s, 2H), 3.81 (s, 6H), 0.21 (s, 9H). ¹³C{¹H} NMR (100 MHz, CDCl₃) δ (ppm): 182.9, 161.3, 157.3, 140.7, 133.5, 130.0, 128.6, 128.2, 120.2, 115.4, 115.0, 114.4, 100.1, 93.2, 56.9, 55.5, -0.10.

2.2.4. Compound **5**

To a solution of compound **4** (105 mg, 0.18 mmol) in THF (4 mL) was added a solution of TBAF in THF (1 M, 180 μL). The solution was stirred at room temperature for 1 hour. Brine (5 mL) was added to the solution and the content was extracted with DCM (4 x 30 mL). The organic layer was dried over anhydrous MgSO₄, filtered and the solvent was removed under vacuum. The crude was filtrated on short column of silica gel with cyclohexane/ethyl acetate (1/9 v:v) as solvent. The obtained orange solid was solubilized in DCM (5 mL), and boron trifluoride etherate (26 μL, 0.21 mmol) was added dropwise to the solution. The reaction mixture was stirred at 40 °C overnight. After cooling, the solvent was removed under vacuum and the crude was purified on silica gel column with cyclohexane/DCM (3/7 v:v) as eluent. Compound **5** was obtained as a red powder (70 mg, 75 %). Mp: 108–109 °C. ¹H NMR (400 MHz, CDCl₃) δ (ppm): 7.01 (d, *J* = 15.4 Hz, 2H), 7.37 (d, *J* = 8.8 Hz, 4H), 7.22 (d, *J* = 8.6 Hz, 2H), 7.10 (d, *J* = 8.7 Hz, 2H), 6.85 (d, *J* = 8.8 Hz, 4H), 6.38 (d, *J* = 15.4 Hz, 2H), 4.80 (d, *J* = 2.4 Hz, 2H), 3.82 (s, 6H), 2.60 (t, *J* = 2.3 Hz, 1H). ¹³C{¹H} NMR (100 MHz, CDCl₃) δ (ppm): 178.0, 162.8, 157.9, 147.3, 133.4, 131.5, 127.5, 125.8, 117.1, 115.5, 115.0, 114.8, 78.4, 76.1, 56.2, 55.7.

2.2.6. DA-*meso*

A mixture of compound **5** (145.0 mg, 0.28 mmol), 1,4-benzoquinone (27.2 mg, 0.25 mmol), CuI (0.5 mg, 0.003 mmol) and PdCl₂(PPh₃)₂ (0.4 mg, 0.0006 mmol) were combined in toluene (5 mL) in a 25 mL Schlenk tube maintained under argon atmosphere. Diisopropyl amine (56 μ L, 0.40 mmol) was added and the reaction was stirred at room temperature for 23 h. The mixture was passed through a short plug of silica, with DCM as eluent, to remove inorganic catalysts. The solvent was removed under vacuum. The crude was purified on silica gel with DCM as eluent, giving **DA-meso** as a red powder (87 mg, 60 %). Mp: 229–230 °C. ¹H NMR (400 MHz, DMSO-d₆) δ (ppm): 7.99 (d, J = 15.5 Hz, 4H), 7.55 (d, J = 8.5 Hz, 8H), 7.32 (d, J = 8.2 Hz, 4H), 7.17 (d, J = 8.2 Hz, 4H), 6.99 (d, J = 8.5 Hz, 8H), 6.39 (d, J = 15.5 Hz, 4H), 5.12 (s, 4H), 3.78 (d, 12H). ¹³C{¹H} NMR (100 MHz, DMSO-d₆) δ (ppm): 177.0, 162.7, 157.2, 146.6, 133.0, 131.5, 126.7, 124.8, 116.5, 115.3, 115.0, 114.9, 76.0, 70.2, 56.0, 55.5. ¹⁹F NMR (376 MHz, DMSO-d₆) δ (ppm): -137.5 (¹⁰B-F, 0.2F), -137.6 (¹¹B-F, 0.8F). (HR-MS (ESI⁺) for (C₆₀H₄₈O₁₀F₄B₂Na⁺) (m/z): Calcd. 1049.3281, found 1049.3273.

2.3. Computational Details

Optimization of the ground state geometries of monomer and dimers **d0**, **d1** and **d2** were performed using DFT with the ω B97X-D exchange–correlation functional [50] and the 6-31+G(d) basis set, as implemented in the Gaussian16 package [51]. Electronic vertical excitations were computed using time-dependent (TD) DFT at the same level of approximation. Diabatic states of **d0-d2** were obtained from adiabatic excited states calculated using the Tamm-Dancoff approximation (TDA) [52] at the ω B97X-D/6-31G(d) level by means of the Boys localization scheme [53], as implemented in Q-Chem [54]. For the diabaticization process, 10, 18 and 24 adiabatic states were considered for **d0**, **d1** and **d2**, respectively.

2.4. Crystallographic structure of **DA-meso**

Dark red single crystals of **DA-meso** could be obtained by slow evaporation of a **DA-meso** solution in DCM/cyclohexane (1/1 v:v) at room temperature. The intensity data for the single-crystal X-ray diffraction analysis were collected on a Rigaku Oxford Diffraction SuperNova diffractometer at room temperature by using Cu/K α radiation ($\lambda = 1.54184 \text{ \AA}$). Data collection reduction and multiscan ABSPACK correction were performed with CrysAlisPro (Rigaku Oxford Diffraction). Using Olex2 [55] the structures were solved by intrinsic phasing methods with SHELXT [56] and SHELXL [57] was used for full matrix least squares refinement. All H-atoms were found experimentally and refined as riding atoms with their Uiso parameters constrained to 1.2Ueq(parent atom) for the CH and CH₂ groups and to 1.5Ueq(parent atom) for the CH₃. CCDC 2169864 for **DA-meso** contains supplementary crystallographic data.

2.5. *Mathematical models used for the description of DA-meso aggregation equilibria*

According to the monomer-dimer model $M + M \rightleftharpoons D (=M_2)$ [58,59], the dimerization constant $K_D = C_D/C_M^2$ can be expressed as $K_D = \frac{1-\alpha_M}{2C_T\alpha_M^2}$ where α_M is the molar fraction of monomer species and $C_T = C_M + 2C_D$ is the total **DA-meso** concentration. Hence, α_M can be expressed as a function of K_D and C_T :

$$\alpha_M = \frac{-1 + \sqrt{8K_D C_T + 1}}{4K_D C_T}$$

The apparent molar absorption coefficient $\varepsilon_{ap} = \varepsilon_M\alpha_M + \varepsilon_D(1-\alpha_M)$ was plotted against C_T . Curve fitting was performed using Igor Pro software from WaveMetrics, which provided calculated values of K_D , α_M , ε_M and ε_D . We also used the isodesmic (equal K) model [59-61] and followed the same procedure taking:

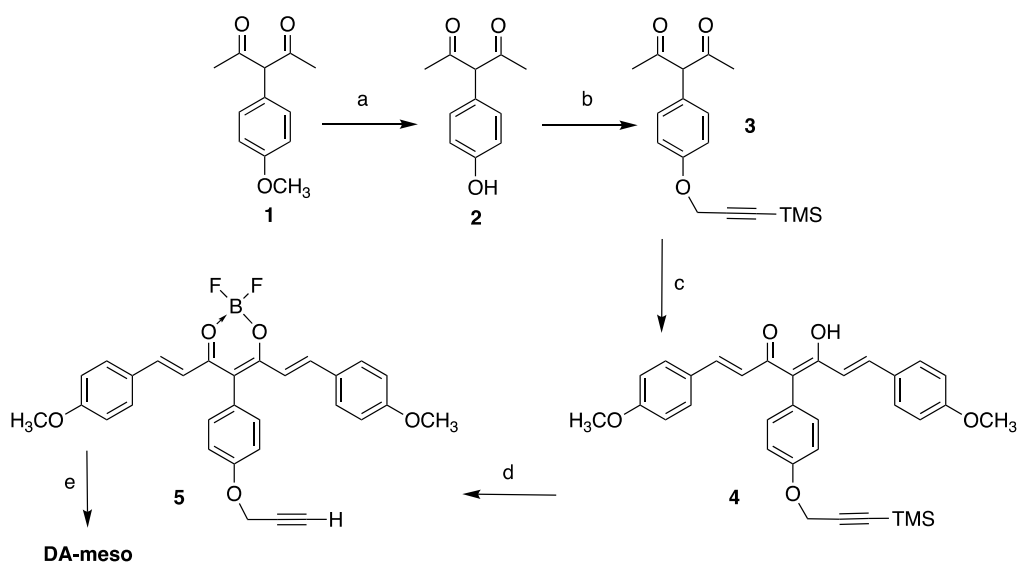
$$\alpha_M = \frac{2KC_T + 1 - \sqrt{4KC_T + 1}}{4K^2C_T^2}$$

3. Results

3.1. Synthesis of *DA-meso*

The synthesis of **R-meso** was described elsewhere [41]. The key precursor in the synthesis of **DA-meso** is 3-(*p*-hydroxyphenyl)-2,4-pentanedione **2** (Scheme 1). According to literature [62], this compound could be obtained directly from CuI/L-proline-catalyzed arylation of acetylacetone. However, the yield of this reaction was found to be low (< 20%) when 4-iodophenol was employed as a reactant. We therefore carried out the same reaction using instead 4-iodoanisole to obtain the *meso* anisole intermediate **1** as described elsewhere [41,62], which was subsequently demethylated with BBr₃ in DCM to afford **2** in two steps with an acceptable overall yield of 49 %. Alkylation of the deprotected phenol function in compound **2** using conventional procedures afforded the propargyl-containing derivative **3**. Claisen-Schmidt condensation of compound **3** with *para*-anisaldehyde was performed using boric acid producing a free curcuminoid intermediate **4**, which was then reacted successively with (*n*-Bu)₄NF and BF₃•etherate to provide curcuminoid-BF₂ **5** [41]. Finally, **DA-meso** molecule was assembled *via* a Glaser coupling of **5** under palladium catalysis in the presence of copper iodide in toluene. **DA-meso** was obtained with an overall yield of 7.5 % from **3** [63]. **DA-meso** was found not soluble enough for recording NMR spectra in chlorinated solvents. It was sparingly soluble in deuterated dimethyl sulfoxide (DMSO-d₆), which enabled recording its proton and heteronuclear NMR spectra. Compared to **R-meso**, the ¹H spectrum of **DA-meso** in DMSO-d₆ revealed no aggregation (Figure S7). The same conclusion was drawn from electrochemical measurements. The cyclic voltammograms recorded in DCM at 5×10⁻⁴ M were consistent with the electrochemical behavior of monochromophoric BF₂-curcuminoids (Figure S11), showing the oxidation and reduction

half-wave potential values ($E^{\circ}_{\text{ox}} = +1.13 \text{ V vs. Fc/Fc}^+$, $E^{\circ}_{\text{red}} = -1.27 \text{ V vs. Fc/Fc}^+$) very close to those obtained for **R-meso** ($E^{\circ}_{\text{ox}} = +1.05 \text{ V vs. Fc/Fc}^+$, $E^{\circ}_{\text{red}} = -1.23 \text{ V vs. Fc/Fc}^+$) [40].



Scheme 1. a) BBr_3 , DCM; b) 3-bromo-1(trimethylsilyl)-1-propyne, K_2CO_3 , acetone; c) 4-methoxybenzaldehyde, B_2O_3 , $(n\text{-BuO})_3\text{B}$, $n\text{-BuNH}_2$, AcOEt; d) $(n\text{-Bu})_4\text{NF}$, THF then $\text{BF}_3\cdot\text{etherate}$, DCM; e) 1,4-benzoquinone, CuI , $\text{PdCl}_2(\text{PPh}_3)_2$, $(i\text{-Pr})_2\text{NH}$, toluene.

3.2. Spectroscopic properties in solution

The spectral and photophysical properties of the monochromophoric reference molecule **R-meso** were reported previously [41]. The UV-vis absorption spectrum of **DA-meso** (conc. 10^{-6} M) in DCM, di(*n*-butyl) ether and diethyl ether matched the absorption profile of **R-meso** (Figure S12) indicating no aggregation in those solvents at this concentration. This observation also confirmed the absence of significant intramolecular interaction between BF_2 -curcuminoid subunits in **DA-meso**, because the stiffness of the bridge forces the two chromophores to lie apart from each other. This is clearly evidenced by the computationally optimized ground state geometry of **DA-meso** (Figure S17).

To monitor the self-assembly of **DA-meso** in solution, we recorded the UV-vis absorption spectra in the apolar solvent cyclohexane (CH) at room temperature as a function

of concentration. The experiments were performed in the concentration range 4.9×10^{-8} M - 2.5×10^{-7} M. Higher concentrations resulted in solute precipitation. Figure 1 shows the concentration-dependent decrease of the **DA-meso** low-energy absorption band peaking at 497 nm and the concomitant appearance of a redshifted (> 520 nm) feature when concentration increases. The presence of a clear isosbestic point at 516 nm indicates the existence of a thermodynamic equilibrium between the bichromophoric monomer and an aggregate. Note that the term monomer refers here to the isolated bichromophoric molecule in equilibrium with aggregate species. Intermolecular aggregation of **DA-meso** is therefore observed to take place at low concentration, the rigid diacetylene bridge imparting the bichromophoric system with a poor solubility in CH and a strong self-association ability. Interestingly, the redshifted spectral feature is similar to that described for **R-Me** and related derivatives in the solid state [20]. It is important to note that the UV-vis absorption spectrum of **R-meso** shows no significant change up to a concentration of 5×10^{-6} M in CH.

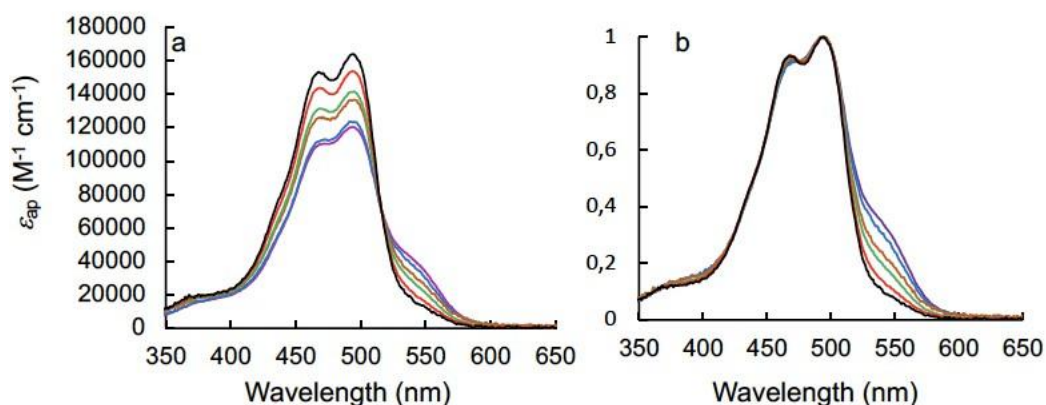


Figure 1. UV-vis absorption spectra of **DA-meso** in CH recorded as a function of dye concentration: 4.92×10^{-8} M (black line), 9.82×10^{-7} M (red), 1.47×10^{-7} M (green), 1.73×10^{-7} M (brown), 2.13×10^{-7} M (blue), 2.46×10^{-7} M (purple); a) apparent molar absorption coefficient, b) same spectra normalized to unity at the absorption maximum (450 nm).

Considering the dimerization model [58,59], we performed a nonlinear regression analysis of the apparent molar absorption coefficient ϵ_{ap} as a function of the total **DA-meso** concentration C_T (Figure 2). The absorbance data were monitored at two wavelengths, 497 nm (monomer) and 545 nm (aggregate). The numerical simulations provided good fits and allowed determining the values of the dimerization constant $K_D = (1.8 \pm 0.3) \times 10^6 \text{ M}^{-1}$ and molar absorption coefficient of the dimer $\epsilon_D = 102\,000 \pm 3400 \text{ M}^{-1}\text{cm}^{-1}$ at 545 nm. The calculated value of the monomer molar absorption coefficient was determined around $160\,000 \text{ M}^{-1}\text{cm}^{-1}$ at 497 nm, which is consistent with about twice the value determined for **R-meso** ($78\,300 \text{ M}^{-1}\text{cm}^{-1}$). To evaluate the possible formation of larger size aggregates, the isodesmic model was also applied to the same set of spectral data [59-61]. Poor fits were obtained (Figure S13) and the analysis performed at the same two wavelengths did not converge toward a unique set of values of K_D , ϵ_M and ϵ_D . Although the occurrence of small amounts of large aggregates in the more concentrated solutions cannot be completely ruled out, we conclude that the major species resulting from **DA-meso** self-assembly is a dimer featuring two self-assembled bis(BF₂-curcuminoid) monomers. As such, the dimer aggregate is a tetrachromophoric system. From the parameters (K_D , ϵ_D) provided by the nonlinear regression analysis, we could calculate the band shape of the UV/Vis absorption spectrum of the dimer aggregate (Figure S14).

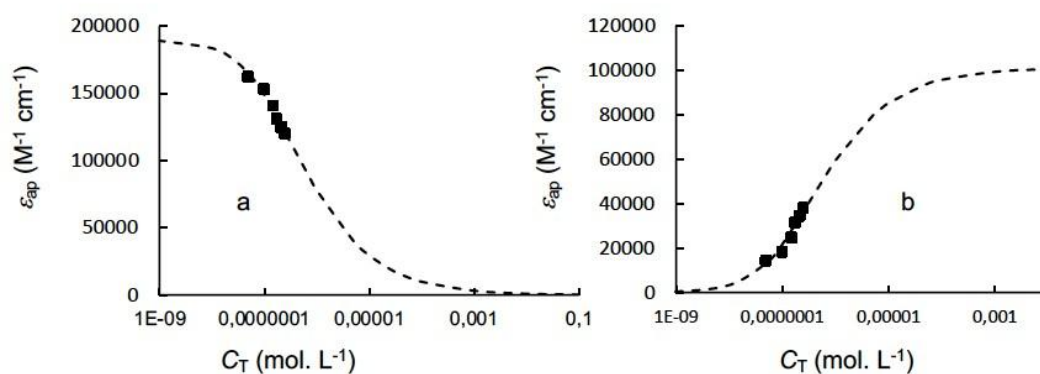


Figure 2. Plot of the apparent molar absorption coefficient against concentration and non-linear regression analysis of the data based on the dimerization model for **DA-meso** in CH at a) 497 nm and b) 525 nm.

The fluorescence emission spectrum of **DA-meso** was measured in CH at 2.46×10^{-7} M. At this concentration, monomer and dimer aggregate coexist with molar fractions of *ca.* 0.4 and 0.6, respectively, as derived from the dimer model calculations. Two different spectral signatures were obtained depending on the excitation wavelength (Figure 3a). A redshifted unstructured emission was observed ($\lambda_{em} = 670 - 700$ nm) upon excitation in the dimer aggregate absorption band at $\lambda_{ex} = 550$ nm. At this wavelength, the absorption of the monomer is negligible. The fluorescence emission quantum yield of the aggregate was found to be low ($\Phi_f = 0.02$) compared to that of the reference compound **R-meso** ($\Phi_f = 0.20$). Exciting the solution at $\lambda_{ex} = 450$ or 470 nm caused the photoexcitation of both monomer and dimer because of the strong overlap of their absorption spectra in this spectral region (Figure S14). A blue-shifted structured fluorescence spectrum (with respect to the dimer aggregate emission) being fairly similar in shape to that of **R-meso** was recorded. However, the fluorescent profile exhibits an emission tail at long wavelengths that can be associated to the emission of the fraction of dimer photoexcited at 450 or 470 nm. As a result, the emission intensity was lower ($\Phi_f = 0.15$) than that of **R-meso** at the same excitation wavelength. Consistently, the fluorescence excitation spectra were found strongly dependent on the observation wavelength (Figure 3b). An aqueous suspension of organic nanoparticles of **R-meso**, prepared according to the fast precipitation method, exhibited UV-vis absorption and fluorescence spectra that resembled that of **R-Me** nanoparticles (Figure S15) [21]. Unlike the case of **DA-meso**, emission and excitation spectra of the colloidal suspensions were not

dependent on excitation and emission wavelengths, respectively, probably due to efficient energy transfer in the condensed phase.

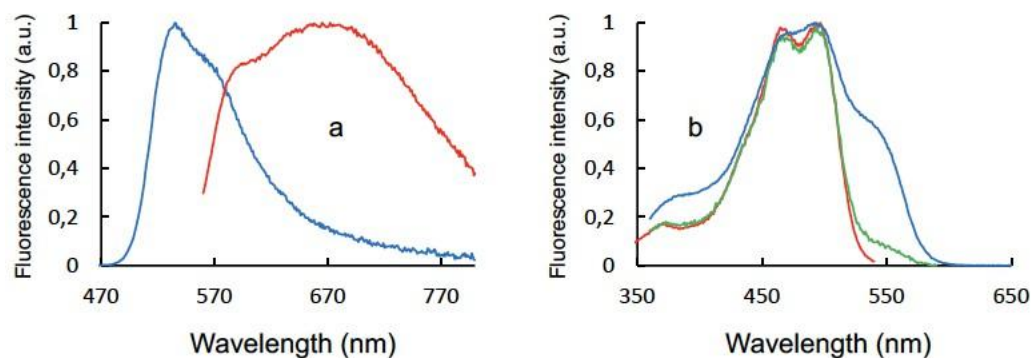


Figure 3. Fluorescence properties of **DA-meso** in CH (2.46×10^{-7} M): a) Emission spectra obtained at $\lambda_{\text{ex}} = 450$ nm (blue) and 550 nm (red). b) Excitation spectra obtained at $\lambda_{\text{em}} = 550$ nm (red), 600 nm (green) and 700 nm (blue).

3.3. Single crystal X-ray diffraction structure analysis

DA-meso compound crystallizes in the monoclinic C2/c space group with only one half molecule in the asymmetric unit, the crystallographic two-fold axis passing through the middle of the dialkyne linker. The molecules adopt a conformation in which the torsional angle between the two propargylic C-O bonds along the dialkyne linker is close to 18° (Figure 4a), which is not the preferential orientation in solution according to DFT calculations (Figure S17). The two curcuminoid-BF₂ units point outwards as they are located on the opposite sides of the average plane formed by the 6-membered linear segment – two propargylic C and four C belonging to the diacetylene linker – and the two phenolic oxygen atoms (Figure 4b).

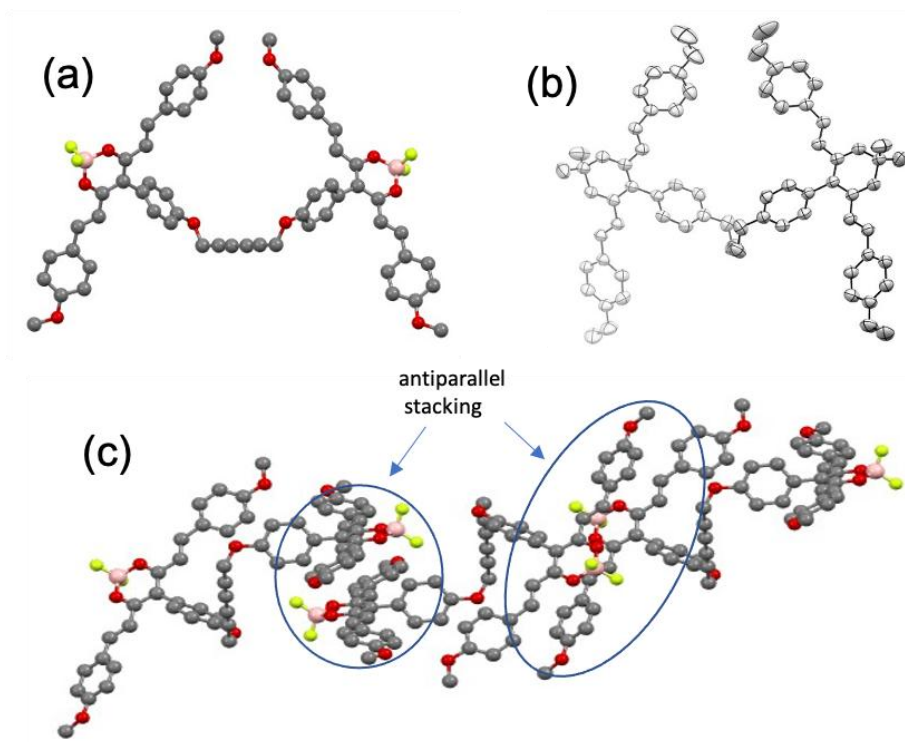


Figure 4. Single-crystal X-ray diffraction structure of **DA-meso**. (a) View perpendicular to the diacetylene axis (b) ORTEP view along the diacetylene axis with ellipsoids drawn at 50% probability level. (c) Three molecules interacting along a molecular thread in the crystal structure of **DA-meso**. Antiparallel stacked fragments indicated with blue circles. Hydrogen atoms are omitted for clarity.

As a consequence, in contrast to the case of other bichromophores connected by a rigid linker [49], such as naphthalene [64], **DA-meso** does form neither a well-defined dimer resulting in a stack of four chromophores nor any kind of discrete supramolecular species in the crystal. Instead, infinite threads are present in the crystal, which can be described as noncovalent polymeric structures. Consistent with previous X-ray structure analyses of BF₂-curcuminoid dyes, we observe that the main intermolecular interaction underpinning the formation of the threads involves the antiparallel stacking of two chromophores (interplanar distance: 3.81 Å) belonging to adjacent **DA-meso** molecules (Figure 4c). We note that the pairs of stacking chromophores interconnecting **DA-meso** molecules in a thread are isolated

from one another (Figure S16). Therefore, unlike the case of monochromophoric BF₂-curcuminoid dyes [21,39,41], the crystal arrangement of **DA-meso** is not characterized by tightly-packed extended stacks of chromophores.

3.4. Molecular aggregation

To gain insights into the molecular and electronic structure of the **DA-meso** dimer in solution, we performed quantum chemical calculations at the ω B97X-D/6-31+G(d) level (see details in the Supporting Information). We considered three possible dimer structures, **d0-d2**, as potential candidates for the molecular dimers in solution. In these structures, the two interacting **DA-meso** molecules are described each by a pair of BF₂-curcuminoid chromophores labelled as A/B and C/D (Figure 5). Dimer **dx** was also included in the study for comparison purposes. It contains two stacked chromophores belonging to two adjacent **DA-meso** molecules (Figure 4c).

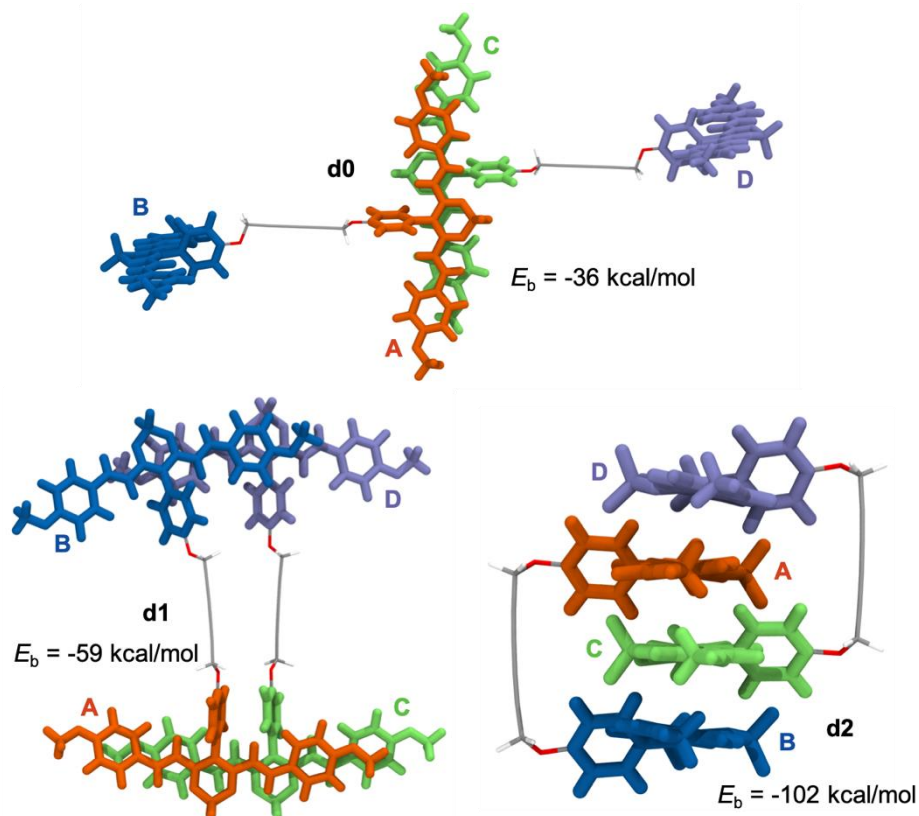


Figure 5. Views of the **d0**, **d1** and **d2** structures showing the chromophore units (A, B, C, D)

In dimer **d0** (Figure 5a, Figure S18), two curcuminoid units A and C are interacting with an antiparallel orientation, the two other ones, B and D, being free. As observed in the crystal, the interacting A-C dimer features a short interplanar distance ($< 3.5 \text{ \AA}$), evidencing the significant role of π -stacking. However, due to the absence of steric constraints, the free chromophore units adopt a perpendicular orientation as calculated for the isolated monomer (Figure S17), which differs from the X-Ray structure **dx**. The electronic binding energy for **d0**, evaluated as $E_b = E(\text{dimer}) - 2E(\text{monomer})$, amounts to -36 kcal/mol .

In the ground state optimized structure of **d1** (Figure 5b, Figure S19), the two **DA-meso** molecules were positioned in such a way that the dye moieties A and B of one molecule interact with those C and D, respectively, of the other molecule. The **d1** geometry thus consists of two independent pairs A-C and B-D of interacting chromophores, in which the constituting BF_2 -curcuminoid moieties interact with their dipole moment aligned in parallel. The A/B molecule presents a *syn* conformation (dihedral angle between A and B chromophores of 57°), whereas the interacting C/D partner adopts an *anti* conformation with a dihedral angle of 127° . The binding energy between the two **DA-meso** molecules in dimer **d1** is equal to -59 kcal/mol , which represents a rather substantial stabilization with respect to **d0**. This is (somehow) unexpected considering that the chromophores in the two interacting pairs A-C and B-D do not adopt the antiparallel stacking commonly found in single crystals of BF_2 -curcuminoid dyes. Unlike dipolar merocyanine dyes [64], PMP-containing BF_2 -curcuminoids display a small permanent dipole moment leading to weak electrostatic intermolecular repulsion in **d1**. In this case, we believe that π -stacking relies for the most part on attractive London dispersion forces. Moreover, this type of arrangement is found in crystals of diacetylenes end-substituted with aromatic groups [48].

Finally, dimer **d2** corresponds to a quadruple stack of chromophores based on two **DA-meso** molecules having a tweezer conformation (Figure 5c, Figure S20). Consistent with the presence of three interacting molecular pairs, the binding energy ($E_b = -102$ kcal/mol) is about three times larger than that calculated for **d0**, which indicates the high stability of the supramolecular structure.

It is worth mentioning that computed binding energies correspond to pristine electronic energy differences, and do not include entropic contributions. The different aggregation modes of dimers suggest that entropy penalty to the binding energy increases as **d0** < **d1** < **d2**. Hence, we expect that thermodynamic stability of dimers (dictated by Gibbs free energies) follow the order dictated by E_b , but with milder differences.

3.5. *Photophysical properties of aggregates*

The **DA-meso** monomer exhibits two degenerate bright excited states at 3.43 eV, corresponding to electronic transitions localized on the two non-interacting chromophore units (Table 1). The lowest-energy excited state (S_1) in dimer **d0** results from the strong coupling between the two stacked monomers A and C. Detailed computational analysis of the electronic transition to S_1 indicates a strong intra-CT character with a vanishing oscillator strength (Tables 1 and S2-S4). At higher energy, the bright state S_5 is localized on the interacting A-C chromophores and displays an important inter-CT character. In between, S_2 - S_4 transitions result from the weak H-type interaction between the two edge chromophores B and D and involve smaller contributions from the A-C sandwich. Accordingly, these three states are degenerate at 3.43 eV, presenting a quasi-pure intra-CT character. A similar state distribution is obtained for dimer **dx**.

Table 1

Energies (in eV) of adiabatic singlet states (oscillator strength in parentheses) of the monomer and dimers **dx** and **d0-2**. States are labelled intra-CT or inter-CT according to its main electronic character.

state	charac.	monomer	dx	d0	d1	d2
S ₁	intra-CT	3.43 (2.35)	3.13 (0.00)	3.03 (0.00)	3.21 (0.00)	2.89 (0.00)
S ₂	intra-CT	3.43 (2.43)	3.36 (2.77)	3.43 (0.26)	3.24 (3.46)	3.06 (0.01)
S ₃	intra-CT		3.40 (0.00)	3.43 (2.52)	3.28 (0.02)	3.23 (0.02)
S ₄	intra-CT		3.49 (5.40)	3.43 (5.01)	3.54 (4.28)	3.40 (1.92)
S ₅	inter-CT		3.77 (0.07)	3.62 (1.08)	3.70 (0.07)	3.45 (0.12)*
S ₆	inter-CT		3.78 (0.00)	3.62 (0.00)	3.72 (0.35)	3.47 (0.35)
S ₇	inter-CT				3.72 (0.05)	3.55 (0.47)
S ₈	inter-CT				3.83 (0.38)	3.58 (2.21)

* Mixed intra-CT/inter-CT character.

A splitting of about 0.3 eV is computed between the two lowest-energy states with strong optical activity in dimer **d1**, where the bright S₂ at 3.24 eV corresponds to excitations within the B and D units, while S₄ (3.54 eV) is associated with excitations on A and C units (Tables 1 and S2, S3, S5). The diabaticization of these low-lying excited states indicates their intra-CT character; namely, they can be described in terms of local excitations from the PMP moieties to the central DOB ring within each constituting curcuminoid. The system can thus be seen as two independent non-equivalent curcuminoid dimers differing by their respective degree of molecular overlap associated to the relative slipping of their constituting units (and, to a lesser extent, their twist). The A-C pair exhibits H-aggregate like behavior, while the B-D dimer shows J-aggregation features, which according the Kasha dipole-dipole model of

interacting chromophores is qualitatively in line with the larger molecular slip within the B-D pair. Exciton couplings related with higher-order transition multipole interactions, e.g., dipole-quadrupole and quadrupole-quadrupole, between chromophoric units are expected to be weaker than the dipole-dipole contribution (Figure S22).

Regarding the nature and energy of the singlet states, a very different picture is obtained for dimer **d2**, in which all four units interact in a quadruple stack and where different effects are expected for central and peripheral components. Three low-lying dark states are found, all exhibiting a local intra-CT character (PMPs and *meso*-phenyl (mPh) to DOB). The first optically allowed state, with computed energy slightly lower than in the monomer (3.40 vs. 3.43 eV), is dominated by inter-CT contributions involving electron density transfer from PMPs and mPh moieties to DOB between pairs of neighboring curcuminoid units (Tables 1 and S2, S3, S6).

4. Discussion

This study shows that linking two BF₂-curcuminoid units through the rigid diacetylene bridge imparts bichromophoric **DA-meso** with a strong ability to self-assemble into a tetrachromophoric dimer in dilute solution. Intermolecular dimerization of **DA-meso** results in UV-vis absorption and fluorescence emission properties similar to those of solid-state BF₂-curcuminoid dyes, which raises the question of the structure of the tetrachromophoric assembly. Because **DA-meso** self-association occurs in a narrow range of very low concentrations ($< 10^{-6}$ M) in CH, solution structure elucidation using NMR experiments was not possible. Single-crystal X-ray diffraction showed the occurrence of extended threads, which are not representative of a solution-phase discrete dimer since the isodesmic model fails to reproduce the concentration-dependent UV-vis absorption data.

Quantum chemical calculations performed on the three possible dimer structures **d0-d2** reveal the presence of a series of excited states close in energy to that of the unperturbed monochromophore, which are not predicted by the classical Frenkel exciton model. This is in agreement with reported theoretical data on quadrupolar-like molecules [16,17,19,31-34]. Especially, low-lying excited states with vanishing oscillator strength are redshifted with respect to the lowest-energy allowed state of the aggregate. Excited-state deactivation toward those dark states could account for the considerably redshifted and low-intensity fluorescence emission of **DA-meso** dimer and, in the more general case, of solid-state aggregates of PMP-containing BF₂-curcuminoid derivatives. Considering the energies of adiabatic excited states, we can see that the energy ordering of singlet states in **d1** exhibits a reasonably good match with the experimental UV-vis absorption spectrum. Especially, the electronic transition to the bright S₂ state in **d1** is found at low energy with a calculated bathochromic shift of 0.19 eV relative to the nonperturbed chromophore in **DA-meso**, consistent with the experimental value found for the position of the long-wavelength shoulder. It is interesting to note that states S₁ to S₄ in **d1** show a quasi-pure intra-CT character. The same remark applies to the low-lying dark states S₁ to S₃ in **d2**, but the first bright excited state, S₄, has here a significant inter-CT parentage and is slightly redshifted relative to the free **DA-meso** compound.

At this stage, it is interesting to compare the results describing the nature of the lowest-energy intra and intermolecular electronic excitations in **DA-meso** with those obtained in a previous study for the dimeric and tetrameric π -stacks of the TPA-containing BF₂-curcuminoid derivative **BF2** [44]. Unlike **DA-meso** dimer, **BF2** aggregates led to low-lying excited states with significant inter-CT parentage and strong inter/intra coupling. The dark inter-CT states in **BF2** were computed at a lower energy than the intra-CT exciton and were demonstrated to be involved in the observed solid-state DF emission. The results obtained with **DA-meso** therefore show a different behavior for PMP-containing BF₂-curcuminoid dyes. Aggregation

results here in redshifted absorption and emission spectra, but DF is not observed because of the absence of such inter-CT states at low energy. The spectral features can be best rationalized by considering the formation of a “non-fluorescent J-aggregate” in **DA-meso** dimer, which is in line with previous conclusions drawn for other quadrupolar-like chromophores [19,20].

Because the computed values of the stabilization enthalpy for **d1** and **d2** are rather large in the gas phase, it is difficult to assign either **d1** or **d2** geometry to the structure of **DA-meso** dimer in solution. We cannot rule out that the increase in concentration of **DA-meso** in CH leads to an interconverting mixture of the three dimers **d0**, **d1**, **d2**. Above a certain concentration threshold, precipitation/crystallization could stir the equilibria toward the formation of **d0** that has a geometry prefiguring the crystalline arrangement **dx**. Single-crystal structures of monochromophoric BF₂-curcuminoids were previously observed to consist of extended columnar π -stacks of cofacially interacting π -conjugated systems with antiparallel dipole moments [21,39,41]. In that respect, the spatial organization of BF₂-curcuminoid units in **d2** would be typical of such arrangement.

5. Conclusion

In summary, this work has shown that **DA-meso** represents a valuable bichromophoric model system to gain insights into the nature of excited states of PMP-containing BF₂-curcuminoid dyes in the solid state. The intermolecular aggregation of **DA-meso** in solution leads to spectral features that are characteristic of the extended arrays found in the crystal, which complements the set of information brought by the flexible bichromophoric counterparts [22,45]. This study also points out the importance of the nature of the electron donor D group on the intra- and inter-CT character of the low-lying excited states of BF₂-curcuminoid dyes in the solid state and, in turn, on thin-film device properties. In that respect,

we believe that the results of this study shed new light on the complex influence of aggregation on the spectral and photophysical properties of curcuminoid-BF₂ dyes, and more generally quadrupolar polarizable dyes.

Author contributions

Claire Tonnelé: DFT calculations, writing original draft. Manon Catherin: syntheses, experimental spectroscopy, titration experiments and curve fittings. Michel Giorgi: acquisition of single-crystal diffraction data and structure resolution. Gabriel Canard: cyclic voltammetry. David Casanova: DFT calculations, writing original draft. Frédéric Castet: DFT calculations, writing original draft. Elena Zaborova: compounds characterizations, writing original draft. Frédéric Fages: writing the manuscript with input from all authors.

Declaration of competing interest

The authors declare that they have no known competing financial interests or personal relationships that could have appeared to influence the work reported in this paper.

Acknowledgements

MC, GC, EZ and FF gratefully acknowledge Aix Marseille Université and CNRS for financial support. The part of the work performed at Aix Marseille Université did not receive any specific grant from funding agencies in the public, commercial, or not-for-profit sectors. CT is supported by DIPC and Gipuzkoa's council joint program Women and Science. CT and DC acknowledge financial support from the Ministerio de Ciencia e Innovación (MICINN) of Spain (projects PID2019-109555GB-I00 and RED2018-102815-T), and the Eusko Jauriaritza/Basque Government (projects PIBA19-0004 and 2019-CIEN-000092-01). CT and DC are thankful for the technical and human support provided by the DIPC Computer Center.

Appendix A. Supplementary data

Supplementary data to this article can be found online at [https://doi.](https://doi.org/)

References

- [1] Bialas, D, Kirchner E, Röhr MIS, Würthner, F. Perspectives in dye chemistry: a rational approach toward functional materials by understanding the aggregate state. *J Am Chem Soc* 2021;143:4500–18. <https://doi.org/10.1021/jacs.0c13245>
- [2] Cornil J, Beljonne D, Calbert JP, Brédas JL. Interchain interactions in organic π -conjugated materials: impact on electronic structure, optical response, and charge transport. *Adv Mater* 2001;13:1053–67. [https://doi.org/10.1002/1521-4095\(200107\)13:14<1053::AID-ADMA1053>3.0.CO;2-7](https://doi.org/10.1002/1521-4095(200107)13:14<1053::AID-ADMA1053>3.0.CO;2-7)
- [3] Curtis MD, Cao J, Kampf JW. Solid-state packing of conjugated oligomers: from π -stacks to the herringbone structure. *J Am Chem Soc* 2004;126:4318–28. <https://doi.org/10.1021/ja0397916>
- [4] Beaujuge PM, Fréchet JMJ. Molecular design and ordering effects in π -functional materials for transistor and solar cell applications. *J Am Chem Soc* 2011;133:20009–29. <https://doi.org/10.1021/ja2073643>
- [5] Anthony JE. Functionalized acenes and heteroacenes for organic electronics. *Chem Rev* 2006;106:5028–48. <https://doi.org/10.1021/cr050966z>
- [6] Banal JL, Zhang B, Jones DJ, Ghiggino KP, Wong WWH. Emissive molecular aggregates and energy migration in luminescent solar concentrators. *Acc Chem Res* 2017;50:49–57. <https://doi.org/10.1021/acs.accounts.6b00432>

- [7] Menke SM, Holmes RJ. Exciton diffusion in organic photovoltaic cells. *Energy Environ Sci* 2014;7:499–512. <https://doi.org/10.1039/C3EE42444H>
- [8] Park KH, Kim W, Yang J, Kim D. Excited-state structural relaxation and exciton delocalization dynamics in linear and cyclic π -conjugated oligothiophenes. *Chem Soc Rev* 2018;47:4279–94. <https://doi.org/10.1039/C7CS00605E>
- [9] Liu J, Zhang H, Dong H, Meng L, Jiang L, Jiang L, Wang Y, Yu J, Sun Y, Hu W, Heeger AJ. High mobility emissive organic semiconductor. *Nat Commun* 2015;6:10032. <https://doi.org/10.1038/ncomms10032>
- [10] Gryn'ova G, Lin KH, Corminboeuf C. Read between the molecules: computational insights into organic semiconductors. *J Am Chem Soc* 2018;140:16370–86. <https://doi.org/10.1021/jacs.8b07985>
- [11] Liu M, Wei Y, Ou Q, Yu P, Wang G, Duan Y, Geng H, Peng Q, Shuai Z, Liao Y. Molecular design strategy for simultaneously strong luminescence and high mobility: multichannel CH- π interaction. *J Phys Chem Lett* 2021;12:938–46. <https://doi.org/10.1021/acs.jpcllett.0c03453>
- [12] D'Avino G, Terenziani F, Painelli A. Aggregates of quadrupolar dyes: giant two-photon absorption from biexciton states. *J Phys Chem B* 2006;110:25590–25592. <https://doi.org/10.1021/jp0673361>
- [13] Spano FC. The spectral signatures of frenkel polarons in H- and J-aggregates. *Acc Chem Res* 2010;43:429–49. <https://doi.org/10.1021/ar900233v>
- [14] Carreras A, Uranga-Barandiaran O, Castet F, Casanova D. Photophysics of molecular aggregates from excited state diabatization. *J Chem Theory Comput* 2019;15:2320–30. <https://doi.org/10.1021/acs.jctc.9b00019>

- [15] Kasha M. Energy transfer mechanisms and the molecular exciton model for molecular aggregates. *Radiat Res* 1963;20:55–70. <https://doi.org/10.2307/3571331>
- [16] Sanyal S, Painelli A, Pati SK, Terenziani T, Sissa C. Aggregates of quadrupolar dyes for two-photon absorption: the role of intermolecular interactions. *Phys Chem Chem Phys* 2016;18:28198–208. <https://doi.org/10.1039/C6CP05153G>
- [17] Zheng C, Zhong C, Collison CJ, Spano FC. Non-Kasha behavior in quadrupolar dye aggregates: the red-shifted H- aggregate. *J Phys Chem C* 2019;123:3203–15. <https://doi.org/10.1021/acs.jpcc.8b11416>
- [18] Zhong C, Bialas D, Collison CJ, Spano FC. Davydov splitting in squaraine dimers. *J Phys Chem C* 2019;123:18734–45. <https://doi.org/10.1021/acs.jpcc.9b05297>
- [19] Bardi B, Dall’Agnese C, Moineau-Chane Ching KI, Painelli A, Terenziani F. Spectroscopic investigation and theoretical modeling of benzothiadiazole-based charge-transfer chromophores: from solution to nanoaggregates. *J Phys Chem C* 2017;121:17466–78. <https://doi.org/10.1021/acs.jpcc.7b04647>
- [20] Bardi B, Dall’Agnese C, Tassé M, Ladeira S, Painelli A, Moineau-Chane Ching KI, Terenziani F. Multistimuli-responsive materials from benzothiadiazole-based charge-transfer chromophores: interdependence of optical properties and aggregation. *ChemPhotoChem* 2018;2:1027–37. <https://doi.org/10.1002/cptc.201800145>
- [21] D’Aléo A, Felouat A, Heresanu V, Ranguis A, Chaudanson D, Karapetyan A, Giorgi M, Fages F. Two-photon excited fluorescence of BF₂ complexes of curcumin analogues: toward NIR-to-NIR fluorescent organic nanoparticles. *J Mater Chem C* 2014;2:5208–15. <https://doi.org/10.1039/C4TC00543K>
- [22] Uranga-Barandiaran O, Catherin M, Zaborova E, D’Aléo A, Fages F, Castet F, Casanova D. Optical properties of quadrupolar and bi-quadrupolar dyes: intra and inter

- chromophoric interactions. *Phys Chem Chem Phys* 2018;20:24623–32. <https://doi.org/10.1039/C8CP05048A>
- [23] Chen G, Sasabe H, Igarashi T, Hong Z, Kido J. Squaraine dyes for organic photovoltaic cells. *J Mater Chem A* 2015;3:14517–34. <https://doi.org/10.1039/C5TA01879J>
- [24] Hou J, Inganäs O, Friend RH, Gao F. Organic solar cells based on non-fullerene acceptors. *Nat Mater* 2018;17:119–28. <https://doi.org/10.1038/nmat5063>
- [25] Susumu K, Fisher JAN, Zheng J, Beratan DN, Yodh AG, Therien MJ. Two-photon absorption properties of proquinoidal D-A-D and A-D-A quadrupolar chromophores. *J Phys Chem A* 2011;115:5525–39. <https://doi.org/10.1021/jp2000738>
- [26] Shimada M, Tsuchiya M, Sakamoto R, Yamanoi Y, Nishibori E, Sugimoto K, Nishihara H. Bright solid-state emission of disilane-bridged donor–acceptor–donor and acceptor–donor–acceptor chromophores. *Angew Chem Int Ed* 2016;128:3074–8. <https://doi.org/10.1002/ange.201509380>
- [27] Mongin O, Porrès L, Charlot M, Katan C, Blanchard-Desce M. Synthesis, fluorescence, and two-photon absorption of a series of elongated rodlike and banana-shaped quadrupolar fluorophores: a comprehensive study of structure–property relationships. *Chem Eur J* 2007;13:1481–98. <https://doi.org/10.1002/chem.200600689>
- [28] Ni W, Wan X, Li M, Wang Y, Chen Y. A–D–A small molecules for solution-processed organic photovoltaic cells. *Chem Commun* 2015;51:4936–50. <https://doi.org/10.1039/C4CC09758K>
- [29] Dereka B, Rosspeintner A, Li Z, Liska R, Vauthey E. Direct Visualization of Excited-State Symmetry Breaking Using Ultrafast Time-Resolved Infrared Spectroscopy. *J Am Chem Soc* 2016;138:4643–49. <https://doi.org/10.1021/jacs.6b01362>

- [30] Chen XK, Kim D, Brédas JL. Thermally activated delayed fluorescence (TADF) path toward efficient electroluminescence in purely organic materials: molecular level insight. *Acc Chem Res* 2018;51:2215–24. <https://doi.org/10.1021/acs.accounts.8b00174>
- [31] Fang F, Zhu L, Li M, Song Y, Sun M, Zhao D, Zhang J. Thermally activated delayed fluorescence material: an emerging class of metal-free luminophores for biomedical applications. *Adv Mater* 2021;8:2102970. <https://doi.org/10.1002/advs.202102970>
- [32] Hestand NJ, Spano FC. Molecular Aggregate Photophysics beyond the Kasha Model: Novel Design Principles for Organic Materials. *Acc Chem Res* 2017;50:341–50. <https://doi.org/10.1021/acs.accounts.6b00576>
- [33] Terenziani F, Painelli A. Supramolecular interactions in clusters of polar and polarizable molecules. *Phys Rev B* 2003;68:165405. <https://doi.org/10.1103/PhysRevB.68.165405>
- [34] Guerrini M, Cocchi C, Calzolari A, Varsano D, Corni S. Interplay between intra- and intermolecular charge transfer in the optical excitations of J- aggregates. *J Phys Chem C* 2019;123:6831–38. <https://doi.org/10.1021/acs.jpcc.8b11709>
- [35] Jursenas S, Gruodis A, Kodis G, Chachisvilis M, Gulbinas V, Silinsh EA, Valkunas L. Free and self-trapped charge-transfer excitons in crystals of dipolar molecules of N,N-dimethylaminobenzylidene 1,3-indandione. *J Phys Chem B* 1998;102:1086–94. <https://doi.org/10.1021/jp971991e>
- [36] Hoffmann M, Schmidt K, Fritz T, Hasche T, Agranovich VM, Leo K. The lowest energy Frenkel and charge-transfer excitons in quasi-one-dimensional structures: application to MePTCDI and PTCDA crystals. *Chem Phys* 2000;258:73–96. [https://doi.org/10.1016/S0301-0104\(00\)00157-9](https://doi.org/10.1016/S0301-0104(00)00157-9)

- [37] Hestand NJ, Spano FC. Expanded theory of H- and J- molecular aggregates: the effects of vibronic coupling and intermolecular charge transfer. *Chem Rev* 2018;118:7069–163. <https://doi.org/10.1021/acs.chemrev.7b00581>
- [38] Kim DH, D'Aléo A, Chen XK, Sandanayaka ASD, Yao D, Zhao L, Komino T, Zaborova E, Canard G, Tsuchiya Y, Choi E, Wu JW, Fages F, Brédas JL, Ribierre JC, Adachi C. High-efficiency electroluminescence and amplified spontaneous emission from a thermally-activated delayed fluorescent near infrared emitter. *Nat Photon* 2018;12:98–104. <https://doi.org/10.1038/s41566-017-0087-y>
- [39] Archet F, Yao D, Chambon S, Abbas M, D'Aléo A, Canard G, Ponce-Vargas M, Zaborova E, Le Guennic B, Wantz G, Fages F. Synthesis of bio-inspired curcuminoid small molecules for solution-processed organic solar cells with high open circuit voltage. *ACS Energy Lett* 2017;2:1303–7. <https://doi.org/10.1021/acsenergylett.7b00157>
- [40] Canard G, Ponce-Vargas M, Jacquemin D, Le Guennic B, Felouat A, Rivoal M, Zaborova E, D'Aléo A, Fages F. Influence of the electron donor groups on the optical and electrochemical properties of borondifluoride complexes of curcuminoid derivatives: a joint theoretical and experimental study. *RSC Adv* 2017;7:10132–42. <https://doi.org/10.1039/C6RA25436E>
- [41] Felouat A, D'Aléo A, Fages F. Synthesis and photophysical properties of difluoroboron complexes of curcuminoid derivatives bearing different terminal aromatic units and a meso-aryl ring. *J Org Chem* 2013;78:4446–4455. <https://doi.org/10.1021/jo400389h>
- [42] Ponce-Vargas M, Štefane B, Zaborova E, Fages F, D'Aléo A, Jacquemin D, Le Guennic B. Searching for new borondifluoride β -diketonate complexes with enhanced

- absorption/emission properties using ab initio tools. *Dyes Pigments* 2018;155:59–67. <https://doi.org/10.1016/j.dyepig.2018.03.022>
- [43] Hao Ye H, Kim DH, Chen XK, Sandanayaka ASD, Kim JU, Zaborova E, Canard G, Tsuchiya Y, Choi E, Wu JW, Fages F, Brédas JL, D'Aléo A, Ribierre JC, Adachi C. Near infrared electroluminescence and low threshold amplified spontaneous emission above 800 nm from a thermally-activated delayed fluorescent emitter. *Chem Mater* 2018;30:6702–10. <https://doi.org/10.1021/acs.chemmater.8b02247>
- [44] Gillett AJ, Tonnelé C, Londi G, Ricci G, Catherin M, Unson DML, Casanova D, Castet F, Olivier Y, Chen WM, Zaborova E, Evans EW, Drummond BH, Conaghan PJ, Cui LS, Greenham NC, Puttison F, Fages F, Beljonne D, Friend RH. Spontaneous exciton dissociation enables spin state interconversion in delayed fluorescence organic semiconductors. *Nat Commun* 2021;12:6640. <https://doi.org/10.1038/s41467-021-26689-8>
- [45] Catherin M, Uranga-Barandiaran O, Brosseau A, Métivier R, Canard G, D'Aléo A, Casanova D, Castet F, Zaborova E, Fages F. Exciton interactions, excimer formation, and $[2\pi+2\pi]$ photodimerization in nonconjugated curcuminoid-BF₂ dimers. *Chem Eur J* 2020;26:3818–28. <https://doi.org/10.1002/chem.201905122>
- [46] Whitlock BJ, Whitlock HW. Concave functionality: design criteria for nonaqueous binding sites. *J Am Chem Soc* 1990;112:3910–5. <https://doi.org/10.1021/ja00166a027>
- [47] Chen CW, Whitlock HW. Molecular tweezers: a simple model of bifunctional intercalation. *J Am Chem Soc* 1978;100:4921–2. <https://doi.org/10.1021/ja00483a063>
- [48] Enkelmann V. Structural aspects of the topochemical polymerization of diacetylene. *Adv Polym Sci* 1984;63:91–136. <https://doi.org/10.1007/BFb0017652>

- [49] Kirchner E, Bialas D, Fennel F, Grüne M, Würthner F. Defined merocyanine dye stacks from a dimer up to an octamer by spacer-encoded self-assembly approach. *J Am Chem Soc* 2019;141:7428–38. <https://doi.org/10.1021/jacs.9b01835>
- [50] Chaia JD, Head-Gordon M. Long-range corrected hybrid density functionals with damped atom–atom dispersion corrections. *Phys Chem Chem Phys* 2008;10:6615–20. <https://doi.org/10.1039/B810189B>
- [51] Frisch MJ, Trucks GW, Schlegel HB, Scuseria GE, Robb MA, Cheeseman JR, Scalmani G, Barone V, Petersson GA, Nakatsuji H, Li X, Caricato M, Marenich AV, Bloino J, Janesko BG, Gomperts R, Mennucci B, Hratchian HP, Ortiz JV, Izmaylov AF, Sonnenberg JL, Williams-Young D, Ding F, Lipparini F, Egidi F, Goings J, Peng B, Petrone A, Henderson T, Ranasinghe D, Zakrzewski VG, Gao J, Rega N, Zheng G, Liang W, Hada M, Ehara M, Toyota K, Fukuda R, Hasegawa J, Ishida M, Nakajima T, Honda Y, Kitao O, Nakai H, Vreven T, Throssell K, Montgomery Jr. JA, Peralta JE, Ogliaro F, Bearpark MJ, Heyd JJ, Brothers EN, Kudin KN, Staroverov VN, Keith TA, Kobayashi R, Normand J, Raghavachari K, Rendell AP, Burant JC, Iyengar SS, Tomasi J, Cossi M, Millam JM, Klene M, Adamo C, Cammi R, Ochterski JW, Martin RL, Morokuma K, Farkas O, Foresman JB, Fox DJ. *Gaussian 16 Rev. B.01* 2016.
- [52] Hirata S, Head-Gordon M. Time-dependent density functional theory within the Tamm–Dancoff approximation. *Chem Phys Lett* 1999;314:291–9. [https://doi.org/10.1016/S0009-2614\(99\)01149-5](https://doi.org/10.1016/S0009-2614(99)01149-5)
- [53] Joseph E, Subotnik JE, Yeganeh S, Cave RJ, Ratner MA. Constructing diabatic states from adiabatic states: Extending generalized Mulliken–Hush to multiple charge centers with Boys localization. *J Chem Phys* 2008;129:244101. <https://doi.org/10.1063/1.3042233>

- [54] Epifanovsky E, Gilbert ATB et al. Software for the frontiers of quantum chemistry: An overview of developments in the Q-Chem 5 package. *J Chem Phys* 2021;155:084801. <https://doi.org/10.1063/5.0055522>
- [55] Dolomanov OV, Bourhis LJ, Gildea RJ, Howard JAK, Puschmann H. OLEX2: a complete structure solution, refinement and analysis program. *J Appl Cryst* 2009;42:339–41. <https://doi.org/10.1107/S0021889808042726>
- [56] Sheldrick GM. Crystal structure refinement with SHELXL. *Acta Cryst* 2015;A71:3–8. <https://doi.org/10.1107/S2053229614024218>
- [57] Sheldrick GM. SHELXT - Integrated space-group and crystal-structure determination. *Acta Cryst* 2015;C71:3–8. <https://doi.org/10.1107/S2053273314026370>
- [58] Lohr A, Grüne M, Würthner F. Self-assembly of bis(merocyanine) tweezers into discrete bimolecular π -stacks. *Chem Eur J* 2009;15:3691–705. <https://doi.org/10.1002/chem.200802391>
- [59] Chen Z, Lohr A, Saha-Möller CR, Würthner F. Self-assembled π -stacks of functional dyes in solution: structural and thermodynamic features. *Chem Soc Rev* 2009;38:564–84. <https://doi.org/10.1039/B809359H>
- [60] Martin RB. Comparisons of indefinite self-association models. *Chem Rev* 1996;96:3043–64. <https://doi.org/10.1021/cr960037v>
- [61] De Greef TFA, Smulders MMJ, Wolffs M, Schenning APHJ, Sijbesma RP, Meijer EW. Supramolecular polymerization. *Chem Rev* 2009;109:5687–754. <https://doi.org/10.1021/cr900181u>

- [62] Jiang Y, Wu N, Wu H, He M. An efficient and mild *cis*-l-proline-catalyzed arylation of acetylacetone or ethyl cyanoacetate. *Synlett* 2005;18:2731–4. <https://doi.org/10.1055/s-2005-918921>
- [63] Yan Q, Zhao D. Conjugated dimeric and trimeric perylenediimide oligomers. *Org Lett* 2009;11:3426–9. <https://doi.org/10.1021/ol9012734>
- [64] Würthner F. Dipole–dipole interaction driven self-assembly of merocyanine dyes: from dimers to nanoscale objects and supramolecular materials. *Acc Chem Res* 2016;49:868–76. <https://doi.org/10.1021/acs.accounts.6b00042>